Inclusive isolated-photon production in pp collisions at $\sqrt{s} = 13$ TeV

A. Cueto, on behalf of the ATLAS Collaboration
Universidad Autónoma de Madrid - Madrid, Spain

Summary. — Measurements of prompt photon production in proton-proton collisions provide a testing ground of perturbative QCD with a hard colourless probe. ATLAS has made public very recently the first measurements of inclusive photon production in the new kinematic regime opened up by the 13 TeV collisions with an integrated luminosity of 3.2 fb^{-1}. The inclusive photon cross section is measured as a function of the photon transverse energy above 125 GeV in different regions of photon pseudorapidity. Next-to-leading-order perturbative QCD and Monte Carlo event-generator predictions are compared to the measured cross sections and provide an adequate description of the data.

1. – Introduction

This article presents a review of the measurement of the cross section for inclusive isolated-photon production in proton-proton collisions at a centre-of-mass energy of 13 TeV [**?**] using the ATLAS detector [**?**].

To perform a test of perturbative QCD (pQCD) only those photons not produced in the decay of neutral mesons are considered in this measurement and referred to as "prompt". At leading order (LO), the production of these photons proceeds via the direct process, in which the photon originates directly from the hard interaction, and the fragmentation process, in which the photon is emitted collinearly to a quark in a fragmentation process [**?**, **?**]. Recent usages of inclusive prompt-photon production measurements comprises studies of novel approaches to the description of parton radiation [**?**], the importance of the resummation of threshold logarithms in QCD and of the electroweak corrections [**?**], and the first calculation of direct photon production at next-to-next-to-leading order (NNLO) [**?**].

Measurements of prompt-photon production at the LHC require isolated photons to avoid the large contribution of photons produced inside jets from hadron decays. After the application of this requirement, the dominant production mechanism in pp collisions is the Compton scattering $qg \to q\gamma$ making these measurements sentitive to the gluon density in the proton [**?**] at LO. Standard Model prompt-photon production represents an important background in searches involving a photon in the final state, therefore, the

improvement of the understanding of prompt-photon production provides an aid to such searches and can be used to tune the Monte Carlo (MC) models.

The inclusive photon cross section is measured as a function of the photon transverse energy (E_T^γ) above 125 GeV in different regions of photon pseudorapidity (η^γ).

2. – Monte Carlo simulations and theoretical predictions

The characteristics of the signal events were studied using simulated events generated with the MC programs Pythia 8.186 [**?**] and Sherpa 2.1.1 [**?**]. Tree-level matrix elements were considered in both generators with the inclusion of initial- and final-state radiation through parton showers.

The signal events included in the Pythia simulation come from both direct processes and photon bremsstrahlung in dijet events. In the Sherpa samples, real higher-order contributions to the Born level photon-plus-jet final state were considered up to three extra partons. To avoid the double counting with the parton shower, the matrix elements and the Sherpa parton shower were merged using the ME+PSLO prescription.

The next-to-leading (NLO) pQCD predictions presented here are computed using the Jetphox 1.3.1_2 progam [**?**, **?**], a parton-level generator which includes a full NLO pQCD calculation of both the direct and fragmentation contributions to the cross section for the $pp \to \gamma +$ X process.

The nominal PDF parametrization used in this calculation is MMHT2014 [**?**] and the NLO photon BFG set II photon fragmentation functions [**?**]. The renormalization μ_R, fragmentation μ_F and factorization scales μ_f are chosen to be $\mu_R = \mu_F = \mu_f = E_T^\gamma$. The strong coupling constant, evaluated at two loops, is set to $\alpha_s(m_Z) = 0.120$. The number of massless quark flavours is set to five.

As the fragementation contribution is taken into account in this calculation, an implementation of a fixed-cone isolation criterion (as imposed at experimental level) can be applied. It requires the total transverse energy from all the partons inside a cone of size $\Delta R = 0.4$ in the $\eta - \phi$ plane around the photon direction to be below $4.2{\times}10^{-3} \times E_T^\gamma + 4.8$ GeV and it is called $E_T^{\mathrm{iso,cut}}$ henceforth.

Corrections to the NLO pQCD predictions for non-perturbative effects coming from residual underlying event (UE) effects and hadronization are consistent with unity within a $\pm 1\%$.

3. – Photon reconstruction and identification

Photon candidates are reconstructed from clusters of energy deposited in the electromagnetic calorimeter (ECAL). A track-matching procedure follows the cluster finding to distinguish between photons and electrons. If no track is found and there is no reconstructed conversion vertex in the inner detector, the candidate is classified as an uncoverted photon. If at least one track is found matched to a conversion vertex consitent to a photon conversion, the candidate is classified as a converted photon. Both

converted and unconverted photons are considered for the measurement.

The characteristics of the energy deposits in the calorimeters are exploited to discriminate signal photons from the hadronic background. The deposits produced by prompt photons in the ECAL are usually narrower and have smaller leakage into the hadronic calorimeter (HCAL) than that of fake photons produced inside jets. The latter ones are also characterized by two separated local maxima in the finely-segmented strips of the first layer of the ECAL. In the first step of the selection, the information from the hadronic calorimeter and the lateral shower shape in the second layer of the ECAL, which contains most of the energy, is used. The final cut-based tight selection comprises tighter cuts on those variables and also places requirements on the shower shapes variables computed from the energy deposits in the first layer.

A further suppression of the background is achived by applying an isolation requirement based on the amount of transverse energy deposited in the cells of both ECAL and HCAL inside a cone of radius $R = 0.4$ in the $\eta - \phi$ plane around the photon candidate, without taking into account the cells within a window of 0.125×0.175 around the photon barycenter. This isolation transverse energy, or simply isolation, is denoted by E_T^{iso}. Two corrections are applied to this value in a event-by-event basis to suppress the photon leakage into the isolation cone and the estimated contributions to E_T^{iso} from the UE and additional inelastic pp interactions (pile-up). After these corrections, E_T^{iso} is required to be lower than $E_T^{\text{iso,cut}}$.

4. – Data selection

The data set used for this measurement was collected with the ATLAS detector during the 25 ns proton-proton collisions running period of 2015, when the LHC operated at a centre-of-mass energy of $\sqrt{s} = 13$ TeV.

Events were recorded using a single-photon high-level trigger, with a nominal transverse energy threshold of 120 GeV. Events are discarded if the calorimeters or inner detector are not fully operational. Reconstructed photon candidates are required to have a transverse momentum greater than 125 GeV. To ensure a proper identification criteria, the photon is limited to the pseudorapidity region covered by the first layer of the ECAL, that is $|\eta^\gamma| < 2.37$ excluding the region $1.37 < |\eta^\gamma| < 1.56$. The photon candidate must be isolated.

In the small fraction of events containing more than one photon candidate satisfying the selection criteria, the highest-E_T^γ (leading) photon is considered.

5. – Signal extraction

Even after the application of identification and isolation criteria, a residual background fraction contaminates the signal region of tight isolated photons. The background yield is estimated and subtracted using a data-driven counting technique, the so-called "two-dimensional sideband method". This method divides the plane formed by the isola-

tion and photon identification variables into a signal region and three background control regions defined as follows:

- A: the signal region containing tight isolated photons.
- B: the non-isolated background region containing tight photons with isolation $E_T^{\rm iso} > E_T^{\rm iso,cut} + 2$ GeV and $E_T^{\rm iso} < 50$ GeV.
- C: the non-tight background region containing non-tight isolated photons.
- D: the background control region containing non-tight photons with isolation $E_T^{\rm iso} > E_T^{\rm iso,cut} + 2$ GeV and $E_T^{\rm iso} < 50$ GeV.

A photon candidate is considered to be non-tight if it fails at least one of the tight requirements on the shower shapes computed from the energy deposits in the first layer of the ECAL, but satisfies all the other tight identification criteria [**?**] and the tight requirement on the total lateral shower width in the first layer of the ECAL.

This method relies on the assumption that the defining variables of the plane are not correlated for the background, so that the following ratio $R^{\rm bg}$ of the number of background events, $N_K^{\rm bg}$ with $K = A, B, C, D$, in the different regions is set to unity for the nominal result.

$$R^{\rm bg} = \frac{N_A^{\rm bg} N_D^{\rm bg}}{N_B^{\rm bg} N_C^{\rm bg}}. \tag{1}$$

The technique also takes into account the signal leakage into the background control regions. The fractions of signal leakage for each region, f_K with $K = B, C, D$ are estimated from the MC simulations of the signal as $f_K = \frac{N_K^{\rm MC}}{N_A^{\rm MC}}$. For each background region, the number of background events is then written as

$$N_K^{\rm bg} = N_K - f_K N_A^{\rm sig}, \tag{2}$$

where N_K is the total number of events in the different regions and $N_A^{\rm sig}$ is the estimated signal yield of tight isolated photons and is inferred from the relation

$$N_A^{\rm sig} = N_A - R^{bg} \frac{(N_B - f_B N_A^{\rm sig})(N_C - f_C N_A^{\rm sig})}{(N_D - f_D N_A^{\rm sig})}. \tag{3}$$

The signal purity, estimated as $\frac{N_A^{\rm sig}}{N_A}$, takes values above 90% for $E_T^\gamma = 125$ GeV, increasing as E_T^γ increases.

6. – Cross-section measurement

The cross section for isolated-photon production is measured as a function of E_T^γ in four regions of η^γ, namely: $|\eta^\gamma| < 0.6$, $0.6 < |\eta^\gamma| < 1.37$, $1.56 < |\eta^\gamma| < 1.81$ and $1.81 < |\eta^\gamma| < 2.37$. After background subtraction, the data distributions are unfolded to particle level, applying bin-by-bin correction factors. These correction factors are

determined using MC samples and take into account the selection efficiency as well as the purity and efficiency of the photon reconstruction. The final diferential cross section is computed for each bin i as

$$\frac{d\sigma}{dE_T^\gamma}(i) = \frac{N_A^{\rm sig}(i) C^{MC}(i)}{\Delta E_T^\gamma(i) \mathcal{L}}, \tag{4}$$

where C^{MC} is the correction factor, ΔE_T^γ is the width of the bin and $\mathcal{L}$ the total integrated luminosity. The cross section measurement procedure is repeated independently for each region of η^γ.

7. – Experimental and theoretical uncertainties

7˙1. *Experimental uncertainties.* – The sources of systematic uncertainties on the cross section measurement are investigated and a total systematic uncertainty is assessed by adding in quadrature the different contributions. The main uncertainties are:

- **photon energy scale and resolution**: assessed using a method developed for the 8 TeV data [**?**] complemented with additional systematic uncertainties to take into account the differences between the 2012 and 2015 data taking periods. The resulting uncertainty increases from approximately 2% at $E_T^\gamma = 125$ GeV to about 5% at $E_T^\gamma \sim 1$ TeV except for the region, $1.56 < |\eta^\gamma| < 1.81$, where it increases from approximately 7% to 18% for the same E_T^γ values.

- **photon identification efficiency**: this uncertainty is estimated from the differences in the shower-shape variables distributions between data an MC simulations. The resulting uncertainty increases from 1–2% at $E_T^\gamma = 125$ GeV to 2–5% at $E_T^\gamma \sim 1$ TeV depending on the η^γ region.

- **correlation between the photon identification variables and isolation**: Following a data-driven method in a background dominated region, a range of $R^{\rm bg}$ is set to cover the observed deviations from unity. The uncertainty on the value $R^{\rm bg} = 1$ is tipically 20% and tends to increase as E_T^γ increases in some regions of η^γ. The resulting uncertainty in the cross section is lower than 2%.

These uncertainties are presented in Figure **??** for each η^γ region.

7˙2. *Theoretical uncertainties.* – The sources of uncertainties considered in the theoretical predictions are:

- The uncertainty due to terms beyond NLO is estimated by the variation of the scale values μ_R, μ_F and μ_f by factors 0.5 and 2 simultaneously or individually. The largest deviation from the nominal value among the 14 variations in each bin is taken as the total uncertainty. This source of uncertainty amounts to 10–15% in all the regions of η^γ and is the dominant source of theoretical uncertainty.

- The uncertainty arising from the imperfect knowledge of the PDF. It increases from 1% at $E_T^\gamma = 125$ GeV to $3-4$% at high E_T^γ.

- The uncertainty due to the value of $\alpha_s(m_Z)$. This uncertainty is below 2%.

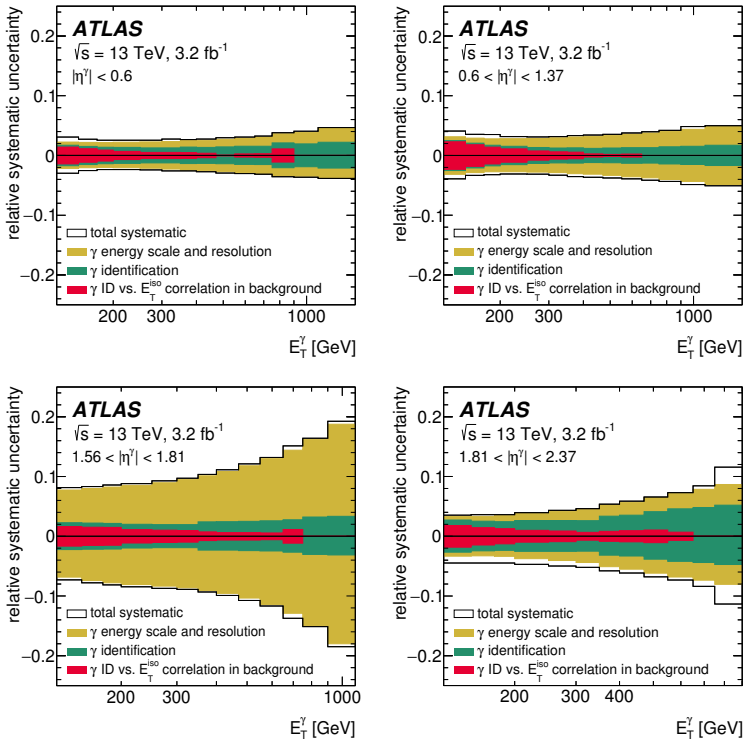

Fig. 1. – Total relative systematic uncertainty in [**?**], excluding that in the luminosity measurement, as a function of E_T^γ for different regions of η^γ as well as the contributions from the photon energy scale and resolution (yellow histogram), the photon identification (green histogram) and the photon identification vs. E_T^{iso} correlation in the background (red histogram). The histograms show the stacked contributions.

- The uncertainty due to the non-perturbative effects is 1%.

The total uncertainty is estimated by adding in quadrature the different sources of uncertainties listed before.

8. – Results

Figure **??** shows the measured cross sections for isolated-photon production as a function of E_T^γ in different regions of the photon pseudorapidity. The measured cross sections span approximately five orders of magnitude in the measured range reaching values of E_T^γ up to 1.5 TeV. No difference in shape is found between different regions of η^γ. The predictions of NLO pQCD calculations of JETPHOX using the MMHT2014 PDF set are compared to the measurement in Figure **??**.

The ratios of the theoretical predictions obtained with different PDF sets are shown in Figure **??** to evaluate better the degree of agreement between theory and data. The differences observed between the predictions based on the MMHT2014, CT14 and NNPDF3.0 PDF sets are much smaller than the theoretical uncertainties. The theoretical uncertain-

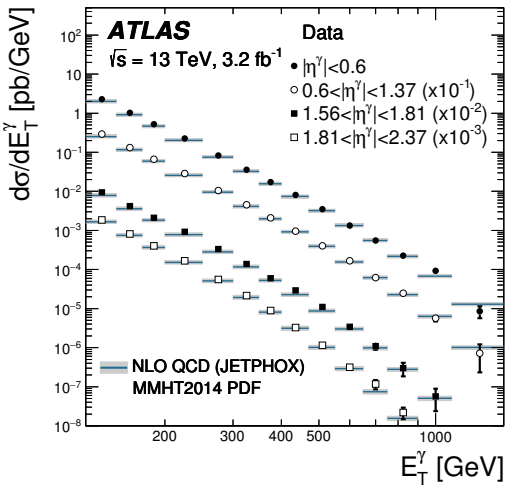

Fig. 2. – Measured cross sections for isolated-photon production as a function of E_T^γ in $|\eta^\gamma| < 0.6$ (black dots), $0.6 < |\eta^\gamma| < 1.37$ (open circles), $1.56 < |\eta^\gamma| < 1.81$ (black squares) and $1.81 < |\eta^\gamma| < 2.37$ (open squares) [**?**]. The NLO pQCD predictions from JETPHOX based on the MMHT2014 PDFs (solid lines) are also shown. The measurements and the predictions are normalized by the factors shown in parentheses to aid visibility. The error bars represent the statistical and systematic uncertainties added in quadrature. The shaded bands display the theoretical uncertainty.

ties are larger than the experimental ones for most of the points of the phase space. The differences between the measurements and the theoretical predictions are 10-15%, being of the same size as the theoretical uncertainties. Therefore, it is concluded that the NLO pQCD predictions provide an adequate description of the measurements.

9. – Conclusions

The measurement of the cross section for inclusive isolated-photon production in pp collisions presented in [**?**] is reviewed. The NLO pQCD predictions of JETPHOX based on different sets of the proton PDFs, provide an adequate description of the data within the experimental and theoretical uncertainties. A combined fit of this measurement together with the measurement of the same process at centre-of-mass energy of 8 TeV [**?**] which takes into account the correlated systematic uncertainties has a stronger constraining power in the evolution of the proton PDFs than either set of measurements alone.

REFERENCES

[1] ATLAS COLLABORATION, arXiv:1701.06882 [hep-ex].
[2] ATLAS COLLABORATION, *JINST*, **3** (2008) S08003.
[3] PIETRYCKI T. and SZCZUREK A., *Phys. Rev. D*, **76** (2007) 034003.

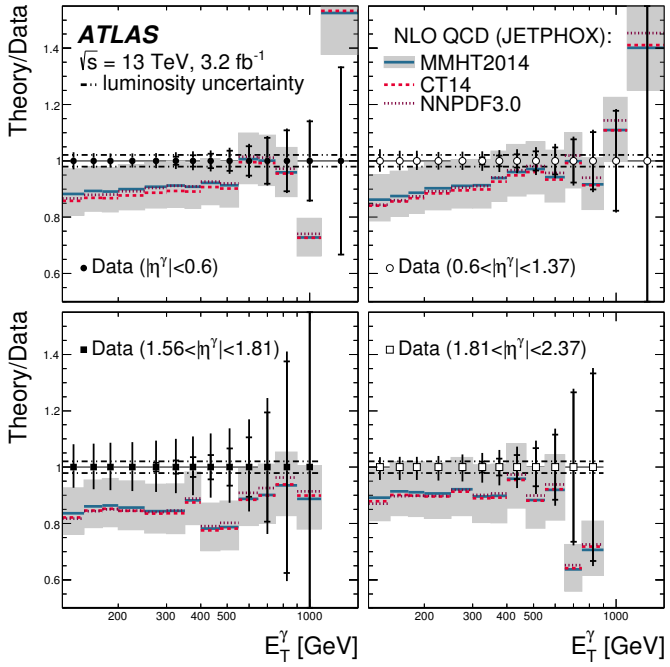

Fig. 3. – Ratio of the NLO pQCD predictions from JETPHOX based on the MMHT2014 PDFs to the measured cross sections for isolated-photon production (solid lines) as a function of E_T^γ in (a) $|\eta^\gamma| < 0.6$, (b) $0.6 < |\eta^\gamma| < 1.37$, (c) $1.56 < |\eta^\gamma| < 1.81$ and (d) $1.81 < |\eta^\gamma| < 2.37$ [**?**]. The inner (outer) error bars represent the statistical uncertainties (statistical and systematic uncertainties, excluding that on the luminosity, added in quadrature), the dot-dot-dashed lines represent the uncertainty due to the luminosity measurement and the shaded bands display the theoretical uncertainty of the calculation based on the MMHT2014 PDFs. The ratio of the NLO pQCD predictions based on the CT14 (dashed lines) or NNPDF3.0 (dotted lines) PDF sets to the data are also included.

[4] BELGHOBSI ET AL., *Phys. Rev. D*, **79** (2009) 114024.
[5] LIPATOV A.V. and MALYSHEV M.A., *Phys. Rev. D*, **94** (2016) 034020.
[6] SCHWARTZ M.D, *JHEP*, **09** (2016) 005.
[7] CAMPBELL J.M, ELLIS R.K. and WILLIAM C., arXiv:1612.04333 [hep-ph].
[8] D'ENTERRIA D. and ROJO J., *Nucl. Phys. B*, **860** (2012) 311.
[9] SJSTRAND T., MRENNA S. and SKANDS P.Z., *Comput. Phys. Commun.*, **178** (2008) 852.
[10] GLEISBERT T. ET AL., *JHEP*, **02** (2009) 007.
[11] AURENCHE P., FONTANNAZ M., GUILLET J.PH., PILON E. and WERLEN M., *Phys. Rev. D*, **73** (2006) 094007.
[12] CATANI S., FONTANNAZ M., GUILLET J.PH. and PILON E., *JHEP*, **05** (2002) 028.
[13] HARLAND-LANG L.A, MARTIN A.D., MOTYLINSKI P. and THORNE R.S, *Eur. Phys. J. C*, **75** (2015) 204.
[14] BOURHIS L., FONTANNAZ M. and GUILLET J.PH., *Eur. Phys. J. C*, **2** (1998) 529.
[15] ATLAS COLLABORATION, *Eur. Phys. J. C*, **76** (2016) 666.
[16] ATLAS COLLABORATION, *Eur. Phys. J. C*, **74** (2014) 3071.
[17] ATLAS COLLABORATION, *JHEP*, **08** (2016) 005.